Valentino Gumbilai,[1] Ken Ebihara,[1,2,3] Megumi Aizawa-Abe,[1,2] Chihiro Ebihara,[1,3] Mingming Zhao,[1] Yuji Yamamoto,[1] Tomoji Mashimo,[4] Kiminori Hosoda,[1,2,5] Tadao Serikawa,[4] and Kazuwa Nakao[1,6]

Fat Mass Reduction With Adipocyte Hypertrophy and Insulin Resistance in Heterozygous PPARγ Mutant Rats

Diabetes 2016;65:2954–2965 | DOI: 10.2337/db15-1422

Agonist-induced activation of peroxisome proliferator–activated receptor-γ (PPARγ) stimulates adipocyte differentiation and insulin sensitivity. Patients with heterozygous PPARγ dominant-negative mutation develop partial lipodystrophy and insulin resistance. Inconsistent with this evidence in humans, it was reported that heterozygous PPARγ knockout mice have increased insulin sensitivity and that mice with heterozygous PPARγ dominant-negative mutation have normal insulin sensitivity and improved glucose tolerance. In the context of the interspecies intranslatability of PPARγ-related findings, we generated a PPARγ mutant rat with a loss-of-function mutation (*Pparg*^{mkyo}) without dominant-negative activity by using the ENU (N-ethyl-N-nitrosourea) mutagenesis method. Heterozygous *Pparg*$^{mkyo/+}$ rats showed reduced fat mass with adipocyte hypertrophy and insulin resistance, which were highly predictable from known actions of PPARγ agonists and phenotypes of patients with the PPARγ mutation. This report is the first in our knowledge to clearly demonstrate that both alleles of PPARγ are required for normal adipocyte development and insulin sensitivity in vivo. Furthermore, the study indicates that PPARγ regulates mainly adipocyte number rather than adipocyte size in vivo. The choice of appropriate species as experimental models is critical, especially for the study of PPARγ.

The nuclear receptor peroxisome proliferator–activated receptor-γ (PPARγ) is a ligand-activated transcription factor that plays an important role as the master regulator for the development of adipocytes (1,2). PPARγ binds to DNA as an obligate heterodimer with the retinoid X receptor and regulates expression of a number of genes related to adipocyte differentiation. The thiazolidinedione (TZD) class of antidiabetic drugs has been shown to be potent in selective ligands for PPARγ (3). Two TZDs, rosiglitazone and pioglitazone, are widely used for the treatment of type 2 diabetes. TZDs are believed to improve insulin sensitivity through the activation of PPARγ. However, the precise mechanism that links PPARγ activity with insulin sensitivity still remains unclear. One of the main reasons for this is that studies using mouse genetic models have shown unexpected phenotypes compared with in vitro experiments and the effect of TZDs in human (4–9).

For the past 25 years, many investigators of medicine and biology have chosen to use mouse models because the technologies involving embryonic stem cells allowed the generation of knockout and knockin mice (10). In 1994, PPARγ was first identified as a central regulator of gene expression and differentiation in adipocytes (11). Since, many in vivo physiological studies on the role of PPARγ in the regulation of adipogenesis and insulin sensitivity have

[1]Department of Medicine and Clinical Science, Kyoto University Graduate School of Medicine, Kyoto, Japan
[2]Institute for Advancement of Clinical and Translational Science, Kyoto University Hospital, Kyoto, Japan
[3]Division of Endocrinology and Metabolism, Jichi Medical University, Tochigi, Japan
[4]Institute of Laboratory Animals, Kyoto University Graduate School of Medicine, Kyoto, Japan
[5]Department of Health and Science, Kyoto University Graduate School of Medicine, Kyoto, Japan
[6]Medical Innovation Center, Kyoto University Graduate School of Medicine, Kyoto, Japan

Corresponding author: Ken Ebihara, kebihara@jichi.ac.jp.

Received 13 October 2015 and accepted 30 June 2016.

This article contains Supplementary Data online at http://diabetes.diabetesjournals.org/lookup/suppl/doi:10.2337/db15-1422/-/DC1.

been done mainly with mouse models (4–9,12–15). However, the results from experiments with mouse genetic models have been inconsistent with human evidence. Although TZDs increase adipocyte differentiation and insulin sensitivity in human (16) and patients with heterozygous PPARγ dominant-negative mutation develop partial lipodystrophy and insulin resistance (17,18), heterozygous PPARγ knockout mice (*Pparg*$^{+/-}$) have increased insulin sensitivity, and mice with heterozygous PPARγ dominant-negative mutation have normal insulin sensitivity and improved glucose tolerance (4–7). On the other hand, rats have a long history in medical research, being fundamental to drug development and advances of physiology and neuroscience. Rats are considered a better model than mice in their physiological and behavioral characteristics, which are sometimes more relevant to humans (19,20). In the current study, we used the N-ethyl-N-nitrosourea (ENU) mutagenesis method (21) to generate a heterozygous PPARγ mutant (*Pparg*$^{mkyo/+}$) rat. *Pparg*^{mkyo} is a missense mutation located in the DNA binding domain that results in a complete loss of function for PPARγ transcriptional activity with no dominant-negative activity against wild-type (WT) PPARγ. Therefore, *Pparg*$^{mkyo/+}$ rat is a de facto PPARγ haploinsufficient model. Through the analysis of *Pparg*$^{mkyo/+}$ rats, this study demonstrates anew that PPARγ positively regulates fat mass and insulin sensitivity. It also reveals that the unexpected phenotypes of mouse models on PPARγ are mouse specific. Furthermore, a novel finding of this study is that PPARγ regulates mainly adipocyte number rather than adipocyte size in vivo. The study demonstrates that the choice of appropriate species as experimental models is critical and that *Pparg*$^{mkyo/+}$ rats are useful for the study of PPARγ.

RESEARCH DESIGN AND METHODS

Animals

Rats with a *Pparg* mutation were obtained by ENU mutagenesis of F344/NSlc rats followed by Mu Transposition Pooling Method With Sequencer (MuT-POWER) screening on the genomic DNA of 4,608 G1 male offspring in Kyoto University Rat Mutant Archive (KURMA). ENU mutagenesis procedures, screening protocols (21), and the intracytoplasmic sperm injection procedure were previously described (22). More than six backcross generations were performed against the F344/NSlc inbred background. Genotyping for *Pparg*^{mkyo} mutation was performed by real-time PCR by using a TaqMan Sample-to-SNP kit (Applied Biosystems, Carlsbad, CA) with a specific primer pair (forward primer sequence 5′-CTGTCGGATC CACAAAAAGAGTAGA-3′ and reverse primer sequence 5′-CCCCACAGCAAGGCACTT-3′) and TaqMan MGB Probes (WT probe sequence 5′-CTGAAACCGACAGTACTG-3′ and mutant probe sequence 5′-CTGAAACCGAAAGTACTG-3′). Genomic DNA was extracted from whole blood. The cycling conditions were 20 s at 95°C followed by 40 cycles of 3 s at 95°C and 20 s at 60°C. Rats were maintained on a 14-h light/10-h dark cycle (lights on 7:00 A.M., lights off 9:00 P.M.) and fed an ad libitum standard pellet diet (MF; Oriental Yeast, Tokyo, Japan). For high-fat diet loading, rats were fed an ad libitum high-fat pellet diet containing 20% weight for weight (wt/wt) protein, 20% wt/wt carbohydrate, and 60% wt/wt fat (D12492; Research Diets, New Brunswick, NJ) from the ages of 8–16 weeks. All animal care and experiments conformed to the Guidelines for Animal Experiments at Kyoto University and were approved by the Animal Research Committee of Kyoto University.

Plasmid Construction, Transfection, and Luciferase Assay

Full-length rat WT PPARγ2 and its C193F mutant cDNA coding sequences were isolated from epididymal adipose tissue total RNA of WT and *Pparg*$^{mkyo/+}$ rats, respectively, by RT-PCR using SuperScript III Reverse Transcriptase kit (Thermo Fisher Scientific, Waltham, MA) and *Pfu* DNA polymerase (Promega, Madison, WI). The WT PPARγ2 and its C193F mutant cDNA fragments were cloned into the pTARGET Mammalian Expression Vector System (Promega) to give pTARGET-WT PPARγ2 and pTARGET-C193F PPARγ2 constructs, respectively. Luciferase assays were performed with a Cignal PPAR Reporter (luc) Kit (QIAGEN) according to the manufacture's protocol. Briefly, to investigate the effect of C193F mutation on PPARγ2 transcriptional activity, pTARGET empty vector, pTARGET-WT PPARγ2, or pTARGET-C193F PPARγ2 was cotransfected with a mixture of PPAR-responsive firefly luciferase reporter and constitutively expressing Renilla construct to human embryonic kidney 293 cells by using Attractene Transfection Reagent (QIAGEN). To investigate the dominant-negative effect of C193F mutant against WT PPARγ2, pTARGET-WT PPARγ2 and pTARGET empty vector or pTARGET-C193F PPARγ2 were cotransfected with reporter mixture. After transfection, cells were incubated at 37°C in a 5% CO_2 incubator for 24 h. The medium was then changed to DMEM containing 10% FBS. After 30 h of transfection, cells were treated with 10 μmol/L pioglitazone (Takeda Pharmaceutical Co., Ltd., Osaka, Japan) or vehicle. After 8 h of treatment, cells were harvested for luciferase assay (Dual-Luciferase Reporter Assay System; Promega).

Chromatin Immunoprecipitation Assay

The 3xFLAG tag DNA fragment was cloned into pTARGET-WT PPARγ2 and pTARGET-C193F PPARγ2 to give pTARGET-3xFLAG-WT PPARγ2 and pTARGET-3xFLAG-C193F PPARγ2. Human embryonic kidney 293 cells were transfected with pTARGET empty vector, pTARGET-3xFLAG-WT PPARγ2, or pTARGET-3xFLAG-C193F PPARγ2 using Lipofectamine reagent (Thermo Fisher Scientific) and were treated with 10 μmol/L pioglitazone for 6 h. Soluble chromatin was immunoprecipitated with anti-FLAG mouse antibody (Merck Millipore, Etobicoke, ON, Canada).

Immunoprecipitates were subjected to quantitative real-time PCR with primer pairs specific to human lipoprotein lipase (LPL) and human perilipin 2 (PLIN2) promoters using KOD SYBR qPCR Mix (TOYOBO CO., LTD, Tokyo, Japan) (LPL promoter forward 5′-GAAAACAGGTGATTGTTGAGT-3′ and reverse 5′-AACGTTTGAGCAAACA-3′; PLIN2 promoter forward 5′-GCAAAAAGAAGCTTGCTCAG-3′ and reverse 5′-TGTTGCCATCTTCAGTGTTT-3′). Quantitative real-time PCR was also performed with the total chromatin input.

Whole-Body Composition Analysis

Sixteen-week-old rats under anesthesia were scanned from nose to anus by computed tomography (CT) with La Theta LCT-100 (Aloka, Tokyo, Japan). The X-ray source tube voltage was set at 50 kV with a constant 1-mA current. Aloka software estimated the volume of adipose tissue, bone, air, and the remainder by using differences in X-ray density. Distinguishing intra-abdominal adipose tissue and subcutaneous adipose tissue was based on detection of the abdominal muscle layers. Fat weight was calculated by using the commonly used density factor of 0.92 g/cm^3. This method provides an accurate estimation of total subcutaneous and intra-abdominal fat pads, as validated by dissection (23).

Adipose Tissue Histology and Adipocyte Size Measurement

Subcutaneous (inguinal), epididymal, and mesenteric fats were sampled from 16-week-old rats, fixed in 10% neutrally buffered formalin, and embedded in paraffin. Histological sections of 5-μm thickness were stained with hematoxylin and eosin and examined by light microscopy. Adipocyte size was evaluated in six rats from each group and six random fields (magnification ×100) per rat. To measure cross-sectional adipocyte area, micrographs were taken with a fluorescent microscope (BioRevo BZ-9000; KEYENCE, Osaka, Japan) and analyzed with Dynamic Cell Count software (KEYENCE).

Liver Histology

Livers were sampled from 16-week-old rats, fixed in 10% neutrally buffered formalin, and embedded in paraffin. Histological sections of 5-μm thickness were stained with hematoxylin and eosin and examined by light microscopy.

Biochemical Assays

Blood was obtained from the tail vein after overnight fasting at the age of 16 weeks. Plasma leptin concentrations were measured by ELISA kit for rat leptin (Millipore, St. Charles, MO). Plasma glucose concentrations were measured by a glucose assay kit (Wako Pure Chemical Industries, Osaka, Japan). Plasma insulin concentrations were measured by an insulin-ELISA kit (Morinaga Institute of Biological Science, Yokohama, Japan). Plasma triglyceride (TG), nonesterified fatty acid (NEFA), and total cholesterol concentrations were measured by enzymatic kits (Triglyceride E-test Wako, NEFA C-test Wako, and Cholesterol E-test Wako, respectively; Wako Pure Chemical Industries). To measure liver and skeletal muscle TG content, we sampled livers and gastrocnemius muscles from 16-week-old rats and immediately froze them in liquid nitrogen. Lipids were extracted with isopropyl alcohol-heptane (1:1 volume for volume). After evaporating the solvent, we resuspended lipids in 99.5% volume for volume ethanol, and TG content was measured by an enzymatic kit (Triglyceride E-test Wako).

Calculation of HOMA of Insulin Resistance

The HOMA of insulin resistance (HOMA-IR) was calculated as an indicator of insulin sensitivity according to Eq. 1:

$$\text{insulin}\,(\mu\text{IU/mL}) \times \text{glucose}\,(\text{mg/dL})/405 \quad \text{(Eq. 1)}$$

Glucose and Insulin Tolerance Tests

Intraperitoneal glucose tolerance test (IPGTT) and intraperitoneal insulin tolerance test (IPITT) were performed after overnight fasting in 16-week-old male rats. For the IPGTT, rats received 2.0 g/kg glucose, and blood was sampled from the tail vein before and 30, 60, and 120 min after the glucose load. For the IPITT, rats received 0.75 IU/kg insulin (Humulin R; Eli Lilly, Indianapolis, IN) by intraperitoneal injection. Blood was sampled from the tail vein before and 30, 60, and 90 min after the insulin load.

Pioglitazone Treatment

Pioglitazone (Wako Pure Chemical Industries) was dissolved in 0.01% carboxymethyl cellulose and administered at doses of 3 mg/kg by oral gavage (0.7 mL) once daily for 8 weeks from the age of 8 weeks in male *Pparg*$^{mkyo/+}$ rats. For vehicle-control animals, the same amount of 0.01% carboxymethyl cellulose was administered.

Real-Time Quantitative RT-PCR

After sampling, tissues were immediately frozen in liquid nitrogen and stored at −80°C until use for RNA isolation. RNA was prepared using TRIzol reagent (Thermo Fisher Scientific) following the manufacturer's protocol. The quality and concentrations of the extracted RNA were checked by using a NanoDrop 2000 spectrophotometer (Thermo Fisher Scientific). Single-stranded cDNA was synthesized from 1 μg of total RNA with the SuperScript III First-Strand Synthesis System (Thermo Fisher Scientific) for RT-PCR according to the manufacturer's instructions. Quantitative RT-PCR was performed with TaqMan (Applied Biosystems) for housekeeping rat mitochondrial subunit 18S rRNA and rat *Pparg* and with SYBR Green (Applied Biosystems) for rat *Fsp27* by the StepOnePlus Real-Time PCR System (Applied Biosystems). The sequences of primers and probe used were as follows: rat 18S forward 5′-GCAATTATTCCCCATGAACGA-3′, rat 18S reverse 5′-CAAAGGGCAGGGACTTAATCAAC-3′, probe 5′-AATTCCCAGTAAGTGCGGGTCATAAGCTTG-3′; rat *Pparg* forward 5′-CCTGCGGAAGCCCTTTGGTGACT-3′, rat *Pparg*

reverse 5′-TGACCAGGGAGTTCCTCAAAA-3′, probe 5′-AG CAAACTCAAACTTAGGCTCCAT-3′; and rat *Fsp27* forward 5′-GTCTCTCAGCCTTCTCTACCC-3′, rat *Fsp27* reverse 5′-CTTGCGCTGTTCTGATGGGG-3′.

Statistical Analysis

Data are expressed as mean ± SEM. Comparison between or among groups was assessed by Student *t* test or ANOVA with Fisher protected least significant difference test. $P < 0.05$ was considered statistically significant.

RESULTS

Generation of PPARγ Mutant Rat and Functional Analysis of Its Mutation

By using ENU mutagenesis followed by MuT-POWER screening of the KURMA samples (21), we generated a heterozygous PPARγ mutant (*Pparg*$^{mkyo/+}$) rat with a missense mutation in *Pparg*. This *Pparg*^{mkyo} mutation, which was G to T transition at nucleotide 488 for PPARγ1 or 578 for PPARγ2, resulted in a substitution of cysteine at codon 163 for PPARγ1 or 193 for PPARγ2 by phenylalanine (C163F or C193F), which is located in the DNA binding domain (Fig. 1*A*). When male and female *Pparg*$^{mkyo/+}$ rats were intercrossed, WT and *Pparg*$^{mkyo/+}$ rats were obtained by a ratio of ~1:2, whereas no homozygous *Pparg*$^{mkyo/mkyo}$ rat was obtained. This result suggests that the *Pparg*$^{mkyo/mkyo}$ mutation was embryonic lethal and that the *Pparg*^{mkyo} mutation had at least some effect on PPARγ function. To investigate the effect of *Pparg*^{mkyo} (C193F) mutation on PPARγ2 transcriptional activity, we performed a luciferase reporter assay (Fig. 1*B* and *C*). Compared with WT PPARγ2, for which the transcriptional activity was appreciably detected at baseline and markedly increased by pioglitazone treatment, the C193F mutant had no significant transcriptional activity with or without pioglitazone, demonstrating that C193F is a complete loss-of-function mutation (Fig. 1*B*). Furthermore, the transcriptional activity of WT PPARγ2 was not affected by the presence of the C193F mutant with or without pioglitazone, demonstrating that the C193F mutant has no dominant-negative activity against WT PPARγ2 (Fig. 1*C*). Because the C193F mutation is located in the DNA binding domain of PPARγ, the effect of C193F

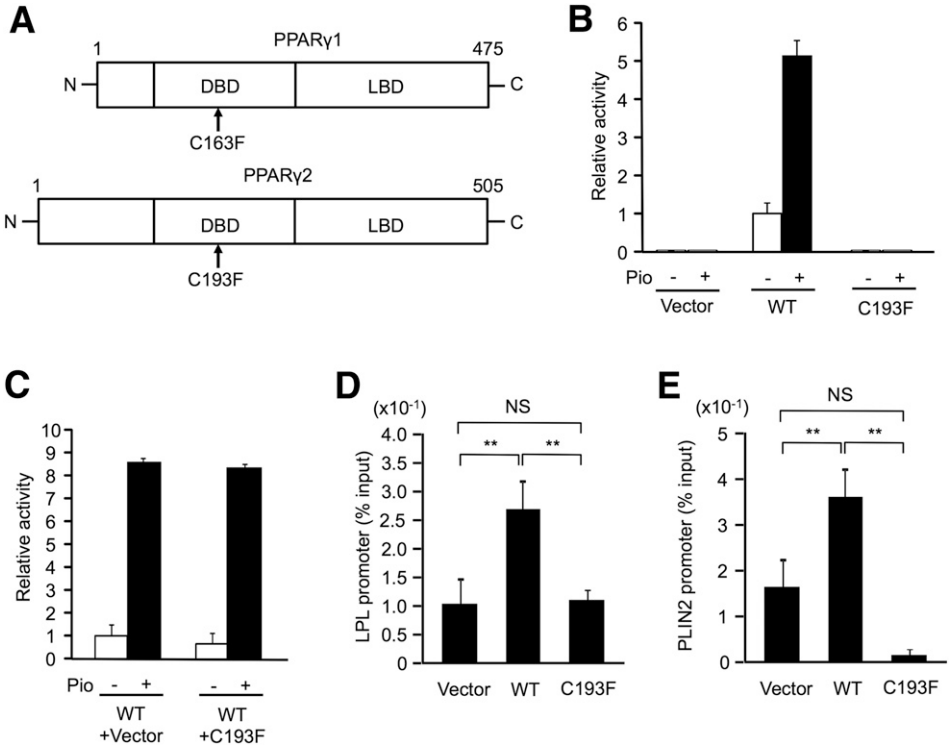

Figure 1—Mutation (C193F) in *Pparg*$^{mkyo/+}$ rats completely disrupts the transcriptional activity of PPARγ2. *A*: Schematic diagrams of PPARγ1 and PPARγ2 that consist of DNA binding domain (DBD) and ligand binding domain (LBD). Arrows indicate the amino acid position of the C163F mutation in PPARγ1 and the C193F mutation in PPARγ2. *B* and *C*: Luciferase assays for the effect of C193F mutation on PPARγ2 transcriptional activity (*B*) and for the dominant-negative effect of C193F mutant against WT PPARγ2 (*C*) with or without pioglitazone (Pio). In these panels, vector indicates pTARGET empty vector; WT, pTARGET-WT PPARγ2 vector; and C193F, pTARGET-C193F mutant PPARγ2 vector. Data are mean ± SEM of three independent experiments. Values obtained with WT PPARγ2 vector (*B*) or WT PPARγ2 vector and empty vector (*C*) without pioglitazone are defined as 1.0. *D* and *E*: Chromatin immunoprecipitation assays for the effect of C193F mutation on PPARγ2 binding on the LPL promoter and PLIN2 promoter. In these panels, vector indicates pTARGET empty vector; WT, pTARGET-3xFLAG-WT PPARγ2 vector; and C193F, pTARGET-3xFLAG-C193F mutant PPARγ2 vector. Soluble chromatin was immunoprecipitated with anti-FLAG mouse antibody. Data are percentage of total chromatin input and mean ± SEM of three independent experiments. $^{**}P < 0.01$ by Student *t* test. NS, not significant.

mutation on PPARγ2 binding on LPL and PLIN2 promoters, including PPARγ-responsive element, was investigated by chromatin immunoprecipitation assay (Fig. 1*D* and *E*). Although binding on both LPL and PLIN2 promoters was observed with WT PPARγ2, no significant binding was detected with C193F PPARγ2 on these promoters compared with results from the empty vector. At this time, WT PPARγ2 and C193F mutant proteins were equally expressed, indicating that C193F mutation does not destabilize the protein (Supplementary Fig. 1). These findings demonstrate that the C193F mutation impairs the DNA binding ability of PPARγ.

Body Weight, Food Intake, and Plasma Leptin Concentration in *Pparg*$^{mkyo/+}$ Rats

No difference in gross appearance between male and female WT and *Pparg*$^{mkyo/+}$ rats fed the standard diet was detected (Fig. 2*A*). Body weight was also unchanged between these groups from birth to age 16 weeks (Fig. 2*B* and *C*). Thus, we fed male and female rats a high-fat diet from the age of 8 weeks. Although the high-fat diet increased body weight in both WT and *Pparg*$^{mkyo/+}$ rats, there was still no significant difference between either group (Fig. 2*D* and Supplementary Fig. 2*A*). Food intake was also unchanged between WT and *Pparg*$^{mkyo/+}$ rats fed the standard and high-fat diets (Fig. 2*E* and Supplementary Fig. 2*B*). In addition, no difference of plasma leptin concentration, an indicator of total body fat, was observed with both the standard and the high-fat diets (Fig. 2*F*).

Total, Subcutaneous, and Intra-abdominal Fat Weights in *Pparg*$^{mkyo/+}$ Rats

Whole-body CT scan was performed to evaluate adiposity in male and female *Pparg*$^{mkyo/+}$ rats. All subcutaneous and intra-abdominal fat weights in *Pparg*$^{mkyo/+}$ rats were slightly, but significantly lower than in WT rats fed the standard diet (Fig. 3*A–C* and Supplementary Fig. 3*A–C*). However, all these differences between WT and *Pparg*$^{mkyo/+}$ rats disappeared with the high-fat diet (Fig. 3*A–C* and Supplementary Fig. 3*A–C*). Weights of epididymal and mesenteric fats, which are the structural components of intra-abdominal fat, were measured directly in both male and female rats. Epididymal fat weight in *Pparg*$^{mkyo/+}$ rats was lower than in WT rats fed the standard and high-fat diets (Fig. 3*D* and Supplementary Fig. 3*D*). On the other hand, no significant difference was found in mesenteric fat weight between WT and *Pparg*$^{mkyo/+}$ rats fed the standard and the high-fat diets (Fig. 3*E* and Supplementary Fig. 3*E*). These results suggest that some difference is present in the effect of PPARγ haploinsufficiency between fat tissues.

Adipocyte Size in *Pparg*$^{mkyo/+}$ Rats

Subcutaneous, epididymal, and mesenteric fats were histologically examined in both male and female rats (Fig. 4*A*

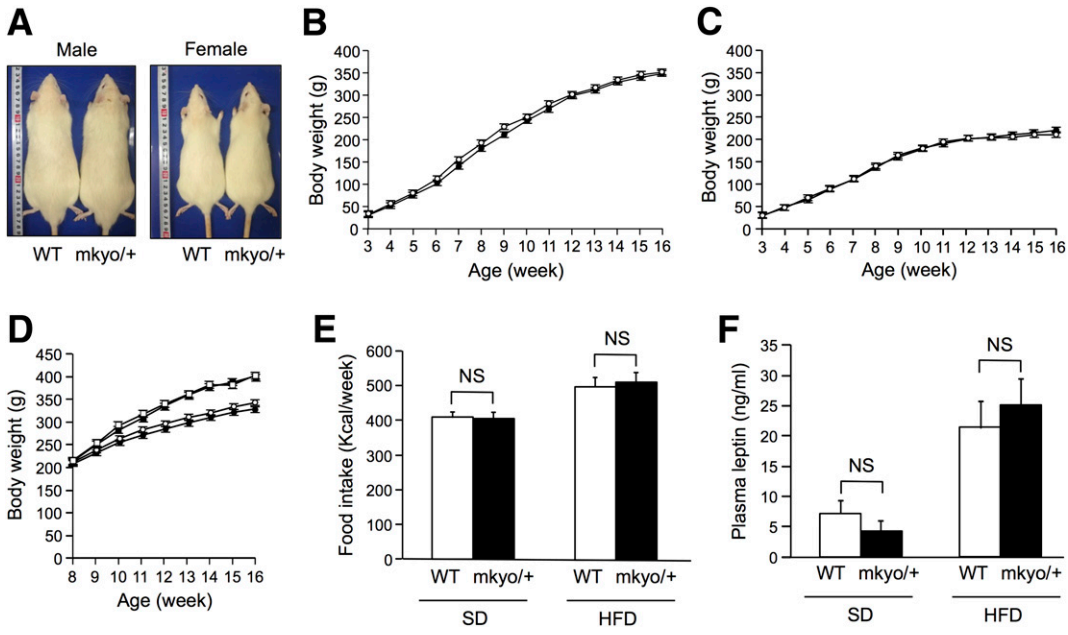

Figure 2—Gross appearance, body weight, food intake, and plasma leptin concentrations of *Pparg*$^{mkyo/+}$ rats. *A*: Gross dorsal view of 16-week-old male and female *Pparg*$^{mkyo/+}$ rats and their WT littermates. *B* and *C*: Growth curves of body weight in male (*B*) and female (*C*) *Pparg*$^{mkyo/+}$ rats (●) and their WT littermates (○) fed a standard diet (SD). Data are mean ± SEM (*n* = 16/group). *D*: Effect of high-fat diet (HFD) on body weight in male *Pparg*$^{mkyo/+}$ rats and their WT littermates. HFD was started at 8 weeks of age. ○, WT rats fed SD; ●, *Pparg*$^{mkyo/+}$ rats fed SD; □, WT rats fed HFD; ■, *Pparg*$^{mkyo/+}$ rats fed HFD. Data are mean ± SEM (*n* = 10/group). *E* and *F*: Food intake and plasma leptin concentration in male *Pparg*$^{mkyo/+}$ rats and their WT littermates fed an SD or HFD. Data are mean ± SEM (*n* = 10/group). NS, not significant (Student *t* test).

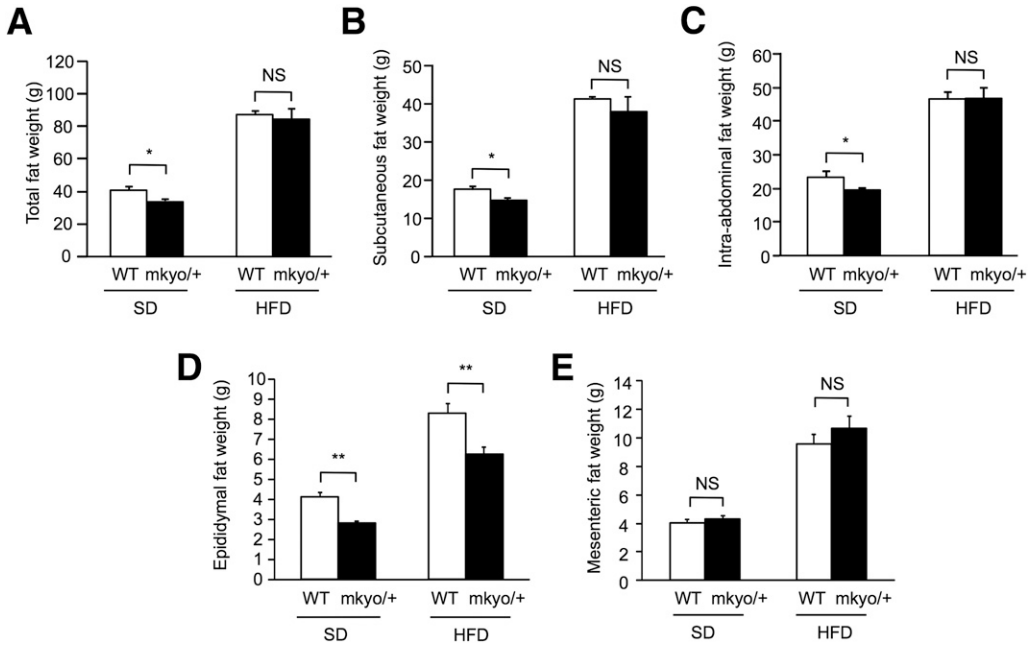

Figure 3—Site-specific fat weight in male *Pparg*$^{mkyo/+}$ rats and their WT littermates fed a standard diet (SD) or high-fat diet (HFD). *A–C*: Weight of total fat, subcutaneous fat, and intra-abdominal fat measured by whole-body CT scan. *D* and *E*: Weight of epididymal fat and mesenteric fat measured directly. Data are mean ± SEM (n = 10/group). *P < 0.05, **P < 0.01 by Student t test. NS, not significant.

and Supplementary Fig. 4*A*). In males, although there was no significant difference in mean cross-sectional adipocyte area of subcutaneous fat between WT and *Pparg*$^{mkyo/+}$ rats fed the standard diet (Fig. 4*B*), that of epididymal and mesenteric fats in *Pparg*$^{mkyo/+}$ rats was significantly larger than in WT rats fed the standard diet (Fig. 4*C* and *D*). With the high-fat diet, mean cross-sectional adipocyte area of all these fats in *Pparg*$^{mkyo/+}$ rats were larger than in WT rats (Fig. 4*B–D*). In female rats, adipocyte area of all fats in *Pparg*$^{mkyo/+}$ rats were significantly larger than in WT rats fed the standard and high-fat diets (Supplementary Fig. 4*B–D*). Even with the standard diet, in all subcutaneous, epididymal, and mesenteric fats, large adipocytes not present in WT rats were observed in *Pparg*$^{mkyo/+}$ rats, and adipocyte size distribution deviated to the right in *Pparg*$^{mkyo/+}$ rats compared with WT rats (Fig. 4*E*). These deviations were more evident with the high-fat diet (Fig. 4*E*).

Induction of Adipocyte Differentiation in Rat Dermal Fibroblasts From *Pparg*$^{mkyo/+}$ Rats

To investigate the effect of PPARγ haploinsufficiency in adipocyte differentiation, we stimulated adipocyte differentiation in rat dermal fibroblasts (RDFs) from WT and *Pparg*$^{mkyo/+}$ rats. Oil red O staining showed that the number of differentiated adipocytes in *Pparg*$^{mkyo/+}$ RDFs was lower than that in WT RDFs (Supplementary Fig. 5). However, pioglitazone treatment increased the number of differentiated adipocytes in both WT and *Pparg*$^{mkyo/+}$ RDFs, and the difference disappeared (Supplementary Fig. 5).

Phenotypes of Liver and Skeletal Muscle in *Pparg*$^{mkyo/+}$ Rats

Although no difference in histological images of the liver between WT and *Pparg*$^{mkyo/+}$ rats was detected with the standard diet, lipid droplets were more noticeable in *Pparg*$^{mkyo/+}$ rats than in WT rats fed the high-fat diet (Fig. 5*A*). Consistent with this, no significant difference in liver weight was found between WT and *Pparg*$^{mkyo/+}$ rats fed the standard diet, but *Pparg*$^{mkyo/+}$ rat livers were significantly heavier than those of WT rats fed the high-fat diet (Fig. 5*B* and Supplementary Fig. 6*A*). Liver TG content was significantly higher in *Pparg*$^{mkyo/+}$ rats, even with the standard diet, and this difference of liver TG content was more evident with the high-fat diet (Fig. 5*C* and Supplementary Fig. 6*B*). Total muscle weight was measured by whole-body CT scan. Although there was no significant difference in total muscle weight between WT and *Pparg*$^{mkyo/+}$ rats fed the standard diet, that in *Pparg*$^{mkyo/+}$ rats was slightly, but significantly heavier than in WT rats fed the high-fat diet (Fig. 5*D* and Supplementary Fig. 6*C*). Gastrocnemius muscle TG content also showed no significant difference with the standard diet but was higher in *Pparg*$^{mkyo/+}$ rats than in WT rats (Fig. 5*E* and Supplementary Fig. 6*D*).

Glucose and Lipid Metabolism in *Pparg*$^{mkyo/+}$ Rats

There was no significant difference in fasting glucose concentration between WT and *Pparg*$^{mkyo/+}$ rats fed the standard and high-fat diets (Fig. 6*A* and Supplementary Fig. 7*A*). However, fasting insulin concentration was significantly higher in *Pparg*$^{mkyo/+}$ rats than in WT rats fed

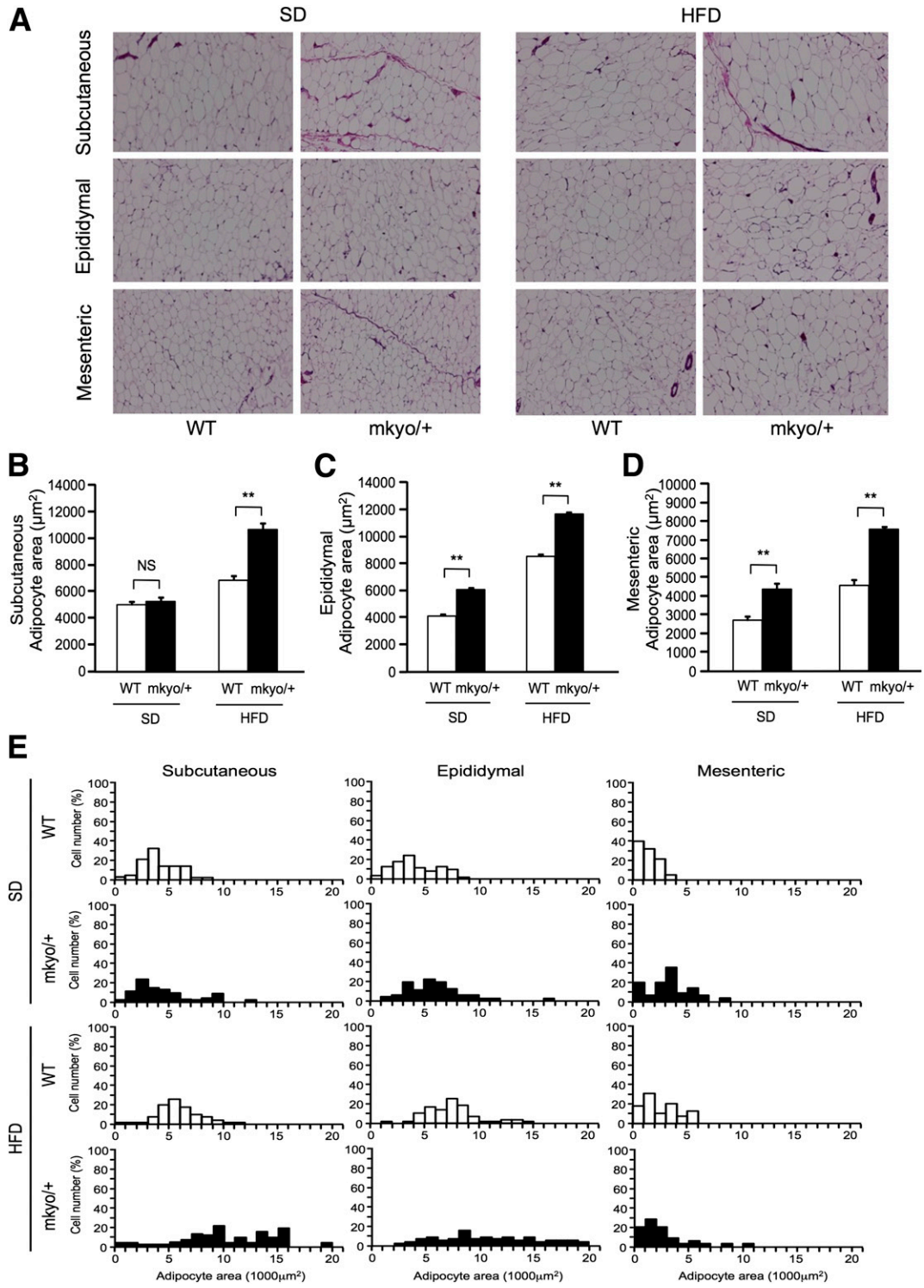

Figure 4—Site-specific adipocyte mean size and size distribution in male *Pparg*$^{mkyo/+}$ rats and their WT littermates fed a standard diet (SD) or high-fat diet (HFD). *A*: Histological images of subcutaneous (inguinal), epididymal, and mesenteric fats. For histological examination, hematoxylin and eosin staining was used (original magnification ×100). *B–D*: Mean cross-sectional area of adipocytes in subcutaneous (inguinal), epididymal, and mesenteric fats. Data are mean ± SEM (n = 10/group). *E*: Adipocyte size distribution in subcutaneous (inguinal), epididymal, and mesenteric fats. $^{**}P < 0.01$ by Student t test. NS, not significant.

the high-fat diet, whereas no significant difference was found with the standard diet (Fig. 6*B* and Supplementary Fig. 7*B*). As a result, HOMA-IR, an indicator of insulin resistance, was significantly higher in *Pparg*$^{mkyo/+}$ rats than in WT rats fed the high-fat diet (Fig. 6*C*). Glucose tolerance examined by IPGTT was worse in *Pparg*$^{mkyo/+}$ rats,

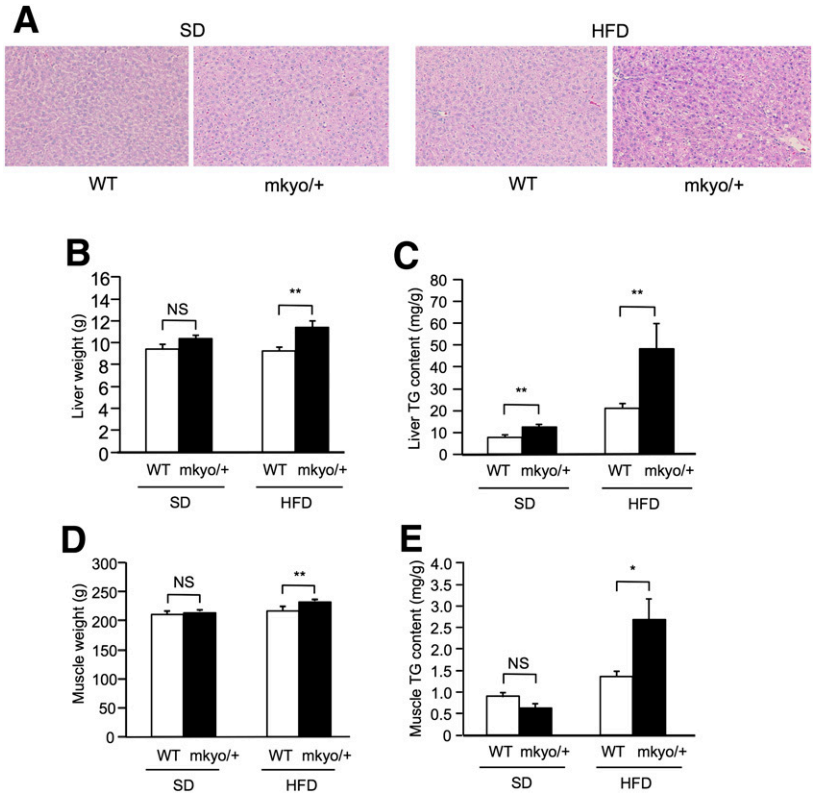

Figure 5—Phenotypes of liver and skeletal muscle in male *Pparg*$^{mkyo/+}$ rats and their WT littermates fed a standard diet (SD) or high-fat diet (HFD). Histological images of the liver (*A*). For histological examination, hematoxylin and eosin staining was used (original magnification ×100). Liver weight (*B*), liver TG content (*C*), and total muscle weight (*D*) measured by whole-body CT scan and TG content in gastrocnemius muscle (*E*). Data are mean ± SEM (n = 10/group). *P < 0.05, **P < 0.01 by Student t test. NS, not significant.

even on the standard diet, and this exacerbation was more evident with the high-fat diet (Fig. 6*D*). Although no significant exacerbation in insulin sensitivity examined by IPITT was detected in *Pparg*$^{mkyo/+}$ rats fed the standard diet, insulin resistance was observed in *Pparg*$^{mkyo/+}$ rats fed the high-fat diet (Fig. 6*E*). Insulin-induced phosphorylation of insulin receptor substrate 1 and Akt was decreased not only in adipose tissues, including subcutaneous, epididymal, and mesenteric fats, but also in liver and skeletal muscle in *Pparg*$^{mkyo/+}$ rats fed the high-fat diet (Supplementary Fig. 8). As to lipid metabolism, no significant difference was found in all plasma TG, NEFA, and total cholesterol concentrations between WT and *Pparg*$^{mkyo/+}$ rats fed the standard and high-fat diets (Fig. 7*A–C* and Supplementary Fig. 7*C*).

Phenotypes of Brown Adipose Tissue in *Pparg*$^{mkyo/+}$ Rats

No difference in gross appearance of interscapular brown adipose tissue (BAT) between WT and *Pparg*$^{mkyo/+}$ rats was detected (Supplementary Fig. 9*A*). BAT weight was also unchanged between WT and *Pparg*$^{mkyo/+}$ rats at baseline (Supplementary Fig. 9*C*). To examine the physiological function of BAT, we conducted a cold exposure experiment. There was no difference in body temperature between WT and *Pparg*$^{mkyo/+}$ rats at baseline (Supplementary Fig. 9*B*). Although 24-h exposure of 4°C decreased the body temperature in both, no difference in body temperature was observed between WT and *Pparg*$^{mkyo/+}$ rats after cold exposure (Supplementary Fig. 9*B*). At this time, BAT weight was similarly decreased in WT and *Pparg*$^{mkyo/+}$ rats (Supplementary Fig. 9*C*). Histological analysis revealed the reduction of lipid content by cold exposure in both WT and *Pparg*$^{mkyo/+}$ rats (Supplementary Fig. 9*D*). In addition, increment of *Ucp1* mRNA expression by cold exposure was similarly observed in these rats (Supplementary Fig. 9*E*). These results indicate that PPARγ haploinsufficiency has little effect on the physiological function of BAT.

Pioglitazone Treatment in *Pparg*$^{mkyo/+}$ Rats

To investigate whether TZD, an agonist of PPARγ can rescue the phenotypes of *Pparg*$^{mkyo/+}$ rats, we treated *Pparg*$^{mkyo/+}$ rats fed the high-fat diet with pioglitazone for 8 weeks. Pioglitazone treatment increased body weight in these rats (Supplementary Fig. 10*A*), and we observed a nonsignificant tendency toward incremental food intake (Supplementary Fig. 10*B*). Total, subcutaneous, and intra-abdominal fat weights measured by CT scan were increased by pioglitazone treatment (Supplementary Fig. 11*A–C*). In direct measurement, epididymal fat weight was also increased, whereas mesenteric fat weight showed no significant increment by pioglitazone treatment (Supplementary

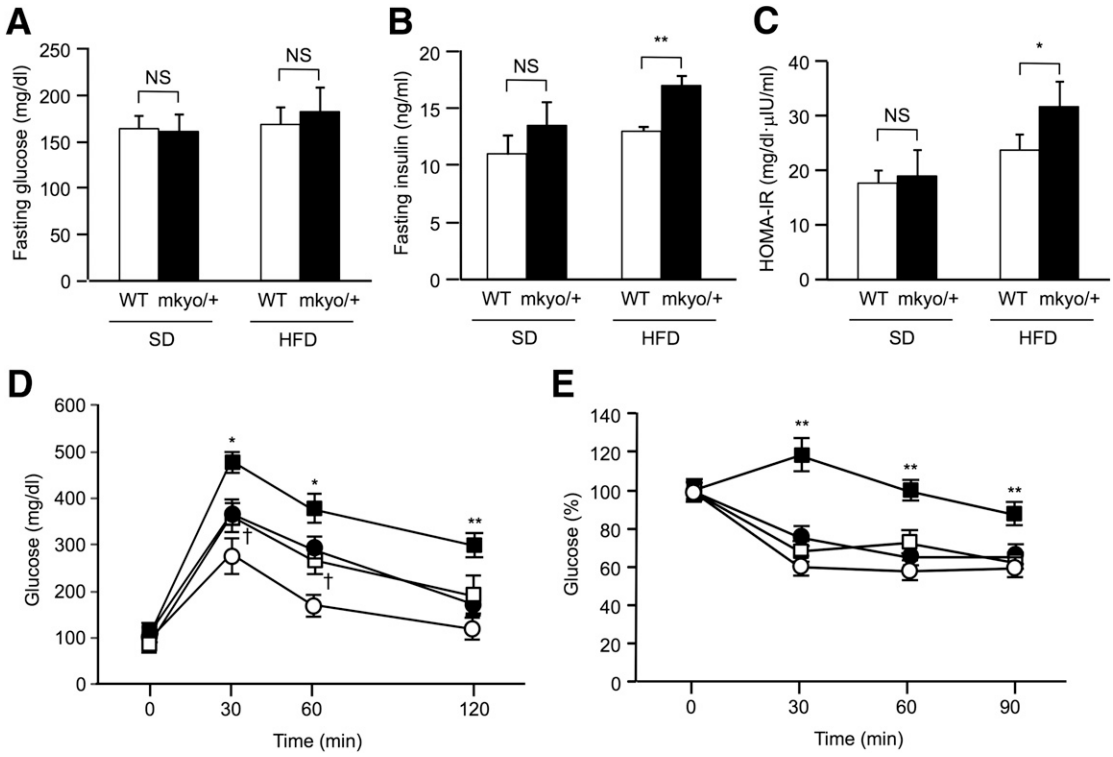

Figure 6—Glucose metabolism in male *Pparg*$^{mkyo/+}$ rats and their WT littermates fed a standard diet (SD) or high-fat diet (HFD). *A–C*: Fasting plasma glucose, fasting plasma insulin concentration, and HOMA-IR. Data are mean ± SEM (n = 10/group). *P < 0.05, **P < 0.01 by Student t test. *D* and *E*: Plasma glucose concentrations during IPGTT and IPITT. ○, WT rats fed SD; ●, *Pparg*$^{mkyo/+}$ rats fed SD; □, WT rats fed HFD; ■, *Pparg*$^{mkyo/+}$ rats fed HFD. Data are mean ± SEM (n = 10/group). *P < 0.05, **P < 0.01 vs. WT rats fed HFD (ANOVA); †P < 0.05 vs. WT rats fed SD (ANOVA). NS, not significant.

Fig. 11*D* and *E*). In histological examination (Supplementary Fig. 12*A*), pioglitazone treatment slightly, but significantly decreased adipocyte area in subcutaneous fat, whereas that in epididymal and mesenteric fats was unchanged (Supplementary Fig. 12*B–D*). Pioglitazone treatment did not affect liver weight and the total muscle weight measured by CT scan but significantly decreased TG content in the liver and skeletal muscle (Supplementary Fig. 13). Pioglitazone treatment significantly decreased fasting glucose and insulin concentrations, indicating that pioglitazone treatment effectively increased insulin sensitivity in *Pparg*$^{mkyo/+}$ rats (Supplementary Fig. 14*A* and *B*). Pioglitazone treatment also decreased fasting TG concentration in *Pparg*$^{mkyo/+}$ rats (Supplementary Fig. 14*C*).

Pparg and *Fsp27* mRNA Expression in Fat Tissues in *Pparg*$^{mkyo/+}$ Rats

To investigate the molecular mechanism by which PPARγ haploinsufficiency affects the phenotype, we examined

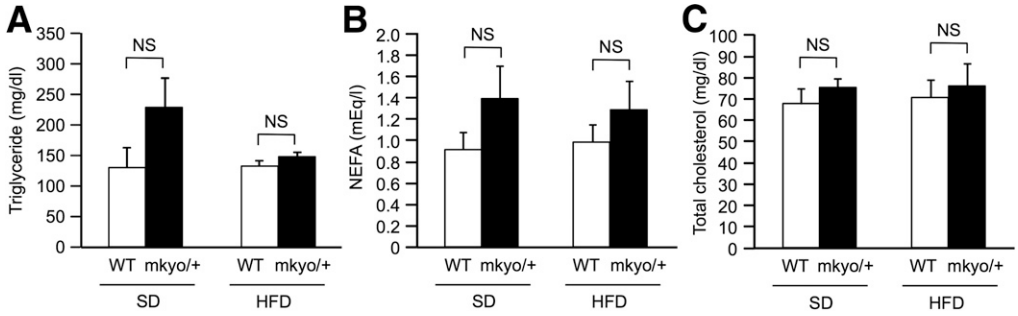

Figure 7—Lipid metabolism in male *Pparg*$^{mkyo/+}$ rats and their WT littermates fed a standard diet (SD) or high-fat diet (HFD). Fasting plasma TG (*A*), fasting plasma TG NEFA (*B*), and fasting plasma total cholesterol (*C*) concentrations. Data are mean ± SEM (n = 10/group). NS, not significant (Student t test).

mRNA expression of PPARγ and its target genes that have the PPARγ responsive element in their promoter, and their expression is regulated by PPARγ in fat tissues, liver, and skeletal muscle in *Pparg*$^{mkyo/+}$ rats (Fig. 8 and Supplementary Figs. 15 and 16). With the standard diet, no significant difference was found in mRNA expression of *Pparg* and its target genes, including *Fsp27*, *Adipoq*, *Cd36*, *Fabp4*, and *Plin1* between WT and *Pparg*$^{mkyo/+}$ rats in any fat tissues (Fig. 8 and Supplementary Figs. 15 and 16). The high-fat diet significantly increased mRNA expression of both *Pparg* and its target genes in all fat tissues in WT rats but did not increase either in any fat tissues in *Pparg*$^{mkyo/+}$ rats (Fig. 8 and Supplementary Figs. 15 and 16). Pioglitazone treatment effectively increased mRNA expression of both *Pparg* and its target genes in all fat tissues in *Pparg*$^{mkyo/+}$ rats fed the high-fat diet (Fig. 8 and Supplementary Figs. 15 and 16). On the other hand, no significant difference was found in mRNA expressions of *Pparg* and its target genes, including *Fsp27* and *Cd36*, in liver and skeletal muscle between WT and *Pparg*$^{mkyo/+}$ rats fed the standard and high-fat diets (Supplementary Fig. 16). Pioglitazone treatment did not increase these mRNA expressions in liver and skeletal muscle (Supplementary Fig. 16).

DISCUSSION

Using gene-driven ENU mutagenesis, we generated a heterozygous PPARγ mutant (*Pparg*$^{mkyo/+}$) rat. *Pparg*^{mkyo} is a missense mutation (C163F for PPARγ1 and C193F for PPARγ2) located in the DNA binding domain (Fig. 1*A*). Luciferase reporter assay revealed that *Pparg*^{mkyo} is a complete loss-of-function mutation at least for its transcriptional activity. Chromatin immunoprecipitation assay revealed that the C193F mutation impaired the DNA binding of PPARγ. When male and female *Pparg*$^{mkyo/+}$ rats were intercrossed, no homozygous *Pparg*$^{mkyo/mkyo}$ rat was obtained, whereas WT and *Pparg*$^{mkyo/+}$ rats were obtained by the expected ~1:2 Mendelian ratio of genotypes. This result suggests that homozygous *Pparg*$^{mkyo/mkyo}$ rat is embryonic lethal. It was previously reported that homozygous PPARγ knockout mouse is embryonic lethal due to placental dysfunction (4), which supports the notion that *Pparg*^{mkyo} is a loss-of-function mutation also in vivo. Furthermore, luciferase reporter assay revealed that the *Pparg*^{mkyo} mutant has no dominant-negative activity against WT PPARγ. Therefore, *Pparg*$^{mkyo/+}$ rat is a de facto PPARγ haploinsufficient model like the *Pparg*$^{+/-}$ mouse.

The mean mutation frequency with ENU mutagenesis of our protocol was one mutation per 3.7 million base pairs (21). Although the chance for the occurrence of an unexpected mutation with a phenotypic effect is relatively small, this possibility also should be taken into account for the experimental design and interpretation of the results. To eliminate mutations that might have been generated by ENU mutagenesis in chromosomal regions other than the *Pparg* locus, we performed a backcross of

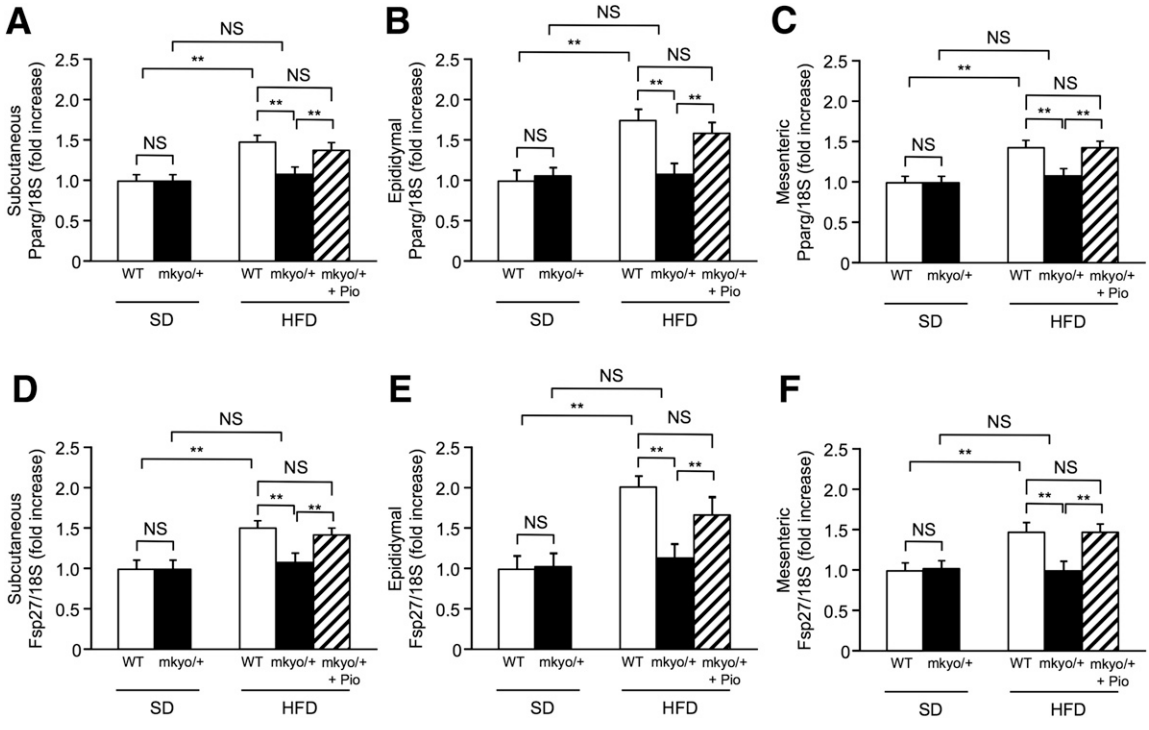

Figure 8—*Pparg* and *Fsp27* mRNA expressions in fat tissues in male *Pparg*$^{mkyo/+}$ rats and their WT littermates fed a standard diet (SD) or high-fat diet (HFD). *A–F*: *Pparg* and *Fsp27* mRNA expressions in subcutaneous (*A* and *D*), epididymal (*B* and *E*), and mesenteric (*C* and *F*) fats. *Pparg*$^{mkyo/+}$ rats fed HFD were treated with pioglitazone (Pio) or vehicle. mRNA expression levels were normalized by 18S rRNA. The fold change is relative to WT rats fed SD. Data are mean ± SEM (n = 5/group). $^{**}P < 0.01$ by Student t test. NS, not significant.

more than six generations against an F344/NSlc inbred background, and we always compared phenotypes between littermates to minimize the effect of possible unexpected mutations.

In this study, the weight of epididymal and mesenteric fats were measured directly. Although epididymal fat weight was reduced, mesenteric fat weight was unchanged in *Pparg*$^{mkyo/+}$ rats compared with WT rats fed both standard and high-fat diets (Fig. 3*D* and *E* and Supplementary Fig. 3*D* and *E*). In patients with familial partial lipodystrophy type 3 (FPLD3, Mendelian Inheritance in Man 604367) that results from heterozygous mutation in *PPARG*, subcutaneous fat mass is reduced, especially in the extremities, whereas intra-abdominal fat mass is preserved (24,25). Consistent with this, treatment with *PPARγ* agonist TZDs generally increases subcutaneous fat mass but decreases intra-abdominal fat mass (26,27). These observations indicate that the effect of PPARγ on adiposity varies with location of fat.

Pparg$^{mkyo/+}$ rats fed both standard and high-fat diets showed adipocyte hypertrophy in subcutaneous, epididymal, and mesenteric fats (Fig. 4 and Supplementary Fig. 4). Although no statistically significant difference of mean adipocyte area in subcutaneous fat of male *Pparg*$^{mkyo/+}$ rats fed a standard diet (Fig. 4*B*) was found, larger adipocytes were detected in subcutaneous fat of male *Pparg*$^{mkyo/+}$ rats, even with a standard diet (Fig. 4*E*). Considering adipocyte hypertrophy with the observation that fat mass was reduced or unchanged in *Pparg*$^{mkyo/+}$ rats, adipocyte number was decreased in *Pparg*$^{mkyo/+}$ rats in all fats examined in this study regardless of diet. The adipocyte hypertrophy observed in *Pparg*$^{mkyo/+}$ rats may be a compensatory response to the decrease in adipocyte number. Treatment with TZDs increases fat mass but decreases mean adipocyte size in human (16), indicating that TZDs increase adipocyte number in human. In the current study, pioglitazone treatment increased fat mass but decreased or did not change adipocyte area in *Pparg*$^{mkyo/+}$ rats (Supplementary Figs. 11 and 12), indicating that pioglitazone treatment increased adipocyte number in rat. Taken together, PPARγ positively regulates adipocyte number in both rat and human.

To investigate the molecular mechanism by which PPARγ haploinsufficiency affects the phenotype of fat tissues, we examined mRNA expression of PPARγ and its target genes in fat tissue, liver, and skeletal muscle in *Pparg*$^{mkyo/+}$ rats (Fig. 8 and Supplementary Figs. 15 and 16). Because the method for analyzing *Pparg* mRNA expression did not discriminate mutant mRNA from WT mRNA, no significant difference was found in *Pparg* mRNA expression between WT and *Pparg*$^{mkyo/+}$ rats fed a standard diet. For PPARγ target genes, we selected *Fsp27*, *Adipoq*, *Cd36*, *Fabp4*, and *Plin1*, which have a PPARγ responsive element in their promoter and in which expression is regulated by PPARγ. The high-fat diet significantly increased mRNA expression of PPARγ target genes in fat tissues in WT rats but did not in *Pparg*$^{mkyo/+}$ rats. Pioglitazone treatment increased mRNA expression of PPARγ target genes in fat tissues even in *Pparg*$^{mkyo/+}$ rats. These observations indicate that the reduction of PPARγ transcriptional activity in fat tissues contribute to the phenotype observed in *Pparg*$^{mkyo/+}$ rats and that pioglitazone treatment rescued the phenotype by increasing PPARγ transcriptional activity in fat tissue. On the other hand, neither PPARγ haploinsufficiency nor pioglitazone treatment affected mRNA expression of PPARγ target genes in liver and skeletal muscle, indicating that liver and muscle are not main sites of PPARγ action in rats.

With the high-fat diet, liver and skeletal muscle TG content was markedly increased in *Pparg*$^{mkyo/+}$ rats compared with WT rats (Fig. 5 and Supplementary Fig. 6) but was not explained by only energy balance because no difference in food intake and total fat mass between WT and *Pparg*$^{mkyo/+}$ rats was found. On the high-fat diet, *Pparg*$^{mkyo/+}$ rats had apparent insulin resistance and hyperinsulinemia (Fig. 6 and Supplementary Fig. 7); thus, hyperinsulinemia possibly contributed to the increase of liver and muscle TG content in *Pparg*$^{mkyo/+}$ rats fed a high-fat diet. Indeed, pioglitazone treatment increased insulin sensitivity and decreased liver and muscle TG content in *Pparg*$^{mkyo/+}$ rats (Supplementary Figs. 13 and 14).

With the standard diet, although there was no statistically significant difference of serum insulin level or HOMA-IR between WT and *Pparg*$^{mkyo/+}$ rats (Fig. 6 and Supplementary Fig. 7), *Pparg*$^{mkyo/+}$ rats showed glucose intolerance by IPGTT compared with WT rats (Fig. 6). With the high-fat diet, *Pparg*$^{mkyo/+}$ rats had significantly increased serum insulin levels, HOMA-IR, and insulin resistance by IPITT (Fig. 6 and Supplementary Fig. 7). Patients with FPLD3, which results from a heterozygous mutation in *PPARG*, show insulin resistance regardless of whether mutations have dominant-negative activity (17,18). These observations indicate that PPARγ haploinsufficiency commonly causes insulin resistance in rat and human. In contrast to PPARγ haploinsufficiency, treatment with TZDs increases adipocyte number and decreases mean adipocyte size (16). In the current study, pioglitazone treatment also increased adipocyte number and insulin sensitivity in *Pparg*$^{mkyo/+}$ rats. The deleterious effect of PPARγ haploinsufficiency on insulin sensitivity might be associated with limited adipocyte number and adipocyte hypertrophy.

Inconsistent with rat and human, it was reported that *Pparg*$^{+/-}$ mice had increased insulin sensitivity (4,5), and mice with a heterozygous PPARγ dominant-negative mutation (*Pparg*$^{P465L/+}$) had normal insulin sensitivity and improved glucose tolerance (6). In *Pparg*$^{+/-}$ mice, although fat mass was reduced like in rat and human, adipocyte size was decreased unlike in rat and human (4). Despite fat mass reduction, *Pparg*$^{+/-}$ mice had hyperleptinemia, which led to suppression of food intake and elevation of body temperature, an index of energy expenditure (4). The negative energy balance brought by hyperleptinemia might keep adipocyte size small. As a result, *Pparg*$^{+/-}$ mice showed increased insulin sensitivity. In *Pparg*$^{P465L/+}$ mice, although adipocyte size was increased like in rat,

subcutaneous fat mass was increased unlike in rat and human (6). *Pparg*$^{P465L/+}$ mice had hyperinsulinemia, which might modify the adiposity and keep insulin sensitivity normal (6). The mechanisms by which *Pparg*$^{+/-}$ mice had hyperleptinemia and *Pparg*$^{P465L/+}$ mice had hyperinsulinemia are unknown, but in mouse, PPARγ plays unexpected physiological roles not observed in rat and human.

In conclusion, this study demonstrates that PPARγ haploinsufficiency causes fat mass reduction, adipocyte hypertrophy, and insulin resistance, which are consistent with the phenotype of patients with heterozygous *PPARG* mutation and the effect of PPARγ agonist TZDs in human, and inconsistent with the phenotypes of *Pparg*$^{+/-}$ mice and heterozygous *Pparg* mutant mice. The choice of appropriate species as experimental models is critical, especially for the study of PPARγ.

Acknowledgments. The authors thank Keiko Hayashi, Department of Medicine and Clinical Science, Kyoto University Graduate School of Medicine, and Norio Sasaoka, Department of Functional Biology, Graduate School of Biostudies, Kyoto University, for technical assistance.

Funding. This work was supported by research grants from the Japanese Ministry of Education, Culture, Sports, Science, and Technology; the Japanese Ministry of Health, Labor and Welfare; and the Uehara Memorial Foundation.

Duality of Interest. No potential conflicts of interest relevant to this article were reported.

Author Contributions. V.G., M.A.-A., and C.E. researched the data and contributed to the discussion and review, editing, and final approval of the manuscript. M.Z. researched the data and contributed to the discussion and review of the manuscript. Y.Y. contributed to the discussion. T.M. and T.S. generated the mutant rat and contributed to the discussion and review of the manuscript. K.H. contributed to the discussion and review of the manuscript. K.N. contributed to the discussion and review, editing, and final approval of the manuscript. K.E. designed the study, researched data, and contributed to the manuscript. K.E. is the guarantor of this work and, as such, had full access to all the data in the study and takes responsibility for the integrity of the data and the accuracy of the data analysis.

References

1. Rosen ED, Walkey CJ, Puigserver P, Spiegelman BM. Transcriptional regulation of adipogenesis. Genes Dev 2000;14:1293–1307
2. Walczak R, Tontonoz P. PPARadigms and PPARadoxes: expanding roles for PPARgamma in the control of lipid metabolism. J Lipid Res 2002;43:177–186
3. Lehmann JM, Moore LB, Smith-Oliver TA, Wilkison WO, Willson TM, Kliewer SA. An antidiabetic thiazolidinedione is a high affinity ligand for peroxisome proliferator-activated receptor gamma (PPAR gamma). J Biol Chem 1995;270:12953–12956
4. Kubota N, Terauchi Y, Miki H, et al. PPAR gamma mediates high-fat diet-induced adipocyte hypertrophy and insulin resistance. Mol Cell 1999;4:597–609
5. Miles PD, Barak Y, He W, Evans RM, Olefsky JM. Improved insulin-sensitivity in mice heterozygous for PPAR-gamma deficiency. J Clin Invest 2000;105:287–292
6. Tsai YS, Kim HJ, Takahashi N, et al. Hypertension and abnormal fat distribution but not insulin resistance in mice with P465L PPARgamma. J Clin Invest 2004;114:240–249
7. Freedman BD, Lee EJ, Park Y, Jameson JL. A dominant negative peroxisome proliferator-activated receptor-gamma knock-in mouse exhibits features of the metabolic syndrome. J Biol Chem 2005;280:17118–17125
8. He W, Barak Y, Hevener A, et al. Adipose-specific peroxisome proliferator-activated receptor gamma knockout causes insulin resistance in fat and liver but not in muscle. Proc Natl Acad Sci U S A 2003;100:15712–15717
9. Jones JR, Barrick C, Kim KA, et al. Deletion of PPARgamma in adipose tissues of mice protects against high fat diet-induced obesity and insulin resistance. Proc Natl Acad Sci U S A 2005;102:6207–6212
10. Vogel G. Nobel prizes. A knockout award in medicine. Science 2007;318:178–179
11. Tontonoz P, Hu E, Graves RA, Budavari AI, Spiegelman BM. mPPAR gamma 2: tissue-specific regulator of an adipocyte enhancer. Genes Dev 1994;8:1224–1234
12. Yamauchi T, Kamon J, Waki H, et al. The mechanisms by which both heterozygous peroxisome proliferator-activated receptor gamma (PPARgamma) deficiency and PPARgamma agonist improve insulin resistance. J Biol Chem 2001;276:41245–41254
13. Imai T, Takakuwa R, Marchand S, et al. Peroxisome proliferator-activated receptor gamma is required in mature white and brown adipocytes for their survival in the mouse. Proc Natl Acad Sci U S A 2004;101:4543–4547
14. Zhang J, Fu M, Cui T, et al. Selective disruption of PPARgamma 2 impairs the development of adipose tissue and insulin sensitivity. Proc Natl Acad Sci U S A 2004;101:10703–10708
15. Medina-Gomez G, Virtue S, Lelliott C, et al. The link between nutritional status and insulin sensitivity is dependent on the adipocyte-specific peroxisome proliferator-activated receptor-gamma2 isoform. Diabetes 2005;54:1706–1716
16. Gealekman O, Guseva N, Gurav K, et al. Effect of rosiglitazone on capillary density and angiogenesis in adipose tissue of normoglycaemic humans in a randomised controlled trial. Diabetologia 2012;55:2794–2799
17. Barroso I, Gurnell M, Crowley VE, et al. Dominant negative mutations in human PPARgamma associated with severe insulin resistance, diabetes mellitus and hypertension. Nature 1999;402:880–883
18. Visser ME, Kropman E, Kranendonk ME, et al. Characterisation of non-obese diabetic patients with marked insulin resistance identifies a novel familial partial lipodystrophy-associated PPARγ mutation (Y151C). Diabetologia 2011;54:1639–1644
19. Aizawa-Abe M, Ebihara K, Ebihara C, et al. Generation of leptin-deficient Lep^{mkyo}/Lep^{mkyo} rats and identification of leptin-responsive genes in the liver. Physiol Genomics 2013;45:786–793
20. Ebihara C, Ebihara K, Aizawa-Abe M, et al. Seipin is necessary for normal brain development and spermatogenesis in addition to adipogenesis. Hum Mol Genet 2015;24:4238–4249
21. Mashimo T, Yanagihara K, Tokuda S, et al. An ENU-induced mutant archive for gene targeting in rats. Nat Genet 2008;40:514–515
22. Hirabayashi M, Kato M, Aoto T, Ueda M, Hochi S. Rescue of infertile transgenic rat lines by intracytoplasmic injection of cryopreserved round spermatids. Mol Reprod Dev 2002;62:295–299
23. Hillebrand JJ, Langhans W, Geary N. Validation of computed tomographic estimates of intra-abdominal and subcutaneous adipose tissue in rats and mice. Obesity (Silver Spring) 2010;18:848–853
24. Savage DB, Tan GD, Acerini CL, et al. Human metabolic syndrome resulting from dominant-negative mutations in the nuclear receptor peroxisome proliferator-activated receptor-gamma. Diabetes 2003;52:910–917
25. Francis GA, Li G, Casey R, et al. Peroxisomal proliferator activated receptor-gamma deficiency in a Canadian kindred with familial partial lipodystrophy type 3 (FPLD3). BMC Med Genet 2006;7:3
26. Kodama N, Tahara N, Tahara A, et al. Effects of pioglitazone on visceral fat metabolic activity in impaired glucose tolerance or type 2 diabetes mellitus. J Clin Endocrinol Metab 2013;98:4438–4445
27. Bi Y, Zhang B, Xu W, et al. Effects of exenatide, insulin, and pioglitazone on liver fat content and body fat distributions in drug-naive subjects with type 2 diabetes. Acta Diabetol 2014;51:865–873